Laser focusing of atoms: a particle-optics approach

J. J. McClelland and M. R. Scheinfein*

Electron and Optical Physics Division, National Institute of Standards and Technology, Gaithersburg, Maryland 20899

Received October 18, 1990; revised manuscript received January 28, 1991

The use of a TEM_{01}*-mode laser beam has been proposed as a means of focusing an atomic beam to nanometer-scale spot diameters. We have analyzed the classical trajectories of atoms through a TEM_{01}*-mode laser beam, using methods developed for particle optics. The differential equation that describes the properties of the first-order paraxial lens has exactly the same form as the bell-shaped magnetic Newtonian lens that was first analyzed by Glaser for the focusing of electrons in an electron-microscope objective. We calculate the first-order properties of the lens, obtaining cardinal elements that are valid over the entire operating range of the lens, including the thick and the immersion regimes. Contributions to the spot size are discussed, including four aberrations plus diffraction and atomic-beam-collimation effects. Explicit expressions for spherical, chromatic, spontaneous-emission, and dipole-fluctuation aberrations are obtained. Examples are discussed for a sodium atomic beam, showing that subnanometer-diameter spots may be achieved with reasonable laser and atomic-beam parameters. Optimization of the lens is also discussed.

1. INTRODUCTION

The influence of near-resonant laser light on the motion of atoms in free space has generated a significant amount of interest over the past few years. In particular it has been suggested and in some ways demonstrated[1-3] that an atomic beam can be focused by using the forces exerted on the atoms by the laser light. The ability to focus atomic beams suggests a number of interesting applications, including atomic microscopy, microfabrication, and precise control of atomic beams for precision measurements. Two major considerations in the practical applicability of laser-controlled atomic focusing are the ease with which the focusing process can be modeled and the ultimate resolution attainable. In this paper we show that for coaxial focusing in a TEM_{01}* laser beam the first-order (paraxial) focal properties can be exactly modeled analytically. We also discuss all the major aberrations in order to show that diffraction-limited spots of the order of 1 nm can in principle be obtained.

An atom in the radiation field of a near-resonant laser experiences two types of force.[4] The spontaneous-emission force results from the absorption and the random spontaneous emission of photons. This random process is limited by the rate at which spontaneous emission occurs, and it saturates as the laser intensity increases. The second type of force, the dipole force, is a result of the interaction of the induced atomic dipole with a gradient in laser-beam intensity. This interaction can be made large by increasing the intensity gradient within the laser beam and by increasing the detuning of the laser frequency from the natural resonance frequency of the atom. In the case of positive detuning, when the laser frequency is greater than the atomic resonance frequency, the force on the atoms is directed from the region of higher laser intensity toward lower laser intensity. The opposite is true for negative detuning; i.e., the force is directed toward higher intensity.

In 1978 Bjorkholm *et al.*[1] demonstrated that an atomic beam that is propagating coaxially with a Gaussian (TEM_{00}) laser beam can be focused to ~250 μm by means of the dipole force. Negative detuning was used, so that the atoms were attracted to the higher laser intensity in the center of the beam. In a subsequent paper[2] Bjorkholm *et al.* showed that a spot size of 28 μm could be obtained, and they examined the limitations on the ultimate spot size that are imposed by spontaneous-emission processes. In 1988 Balykin *et al.*[3] reported experiments with a lens made up of two counterpropagating, diverging, Gaussian laser beams that were oriented transversely to the atomic beam. They were able to obtain the image of two atomic sources, demonstrating real image formation with a laser atomic lens. While these experiments represent important pioneering work, both methods of focusing atoms suffer from the same problem if one is concerned with the ultimate resolution. In each case the atoms travel through regions of high laser intensity, where a significant amount of spontaneous emission occurs. This emission acts to increase the amount of random motion in the atomic beam, which effectively decreases the resolution.

Balykin and Letokhov[5] first analyzed the properties of a laser atomic lens that consists of an atomic beam traveling coaxially through the focus of a TEM_{01}* laser beam (see Fig. 1). Positive detuning is used, so the force is directed toward the hollow center of the laser beam. This type of lens has the advantage that the atoms go through a relatively low-intensity region, so spontaneous emission is kept to a minimum. Balykin and Letokhov treated the lens according to the thin-lens approximation and analyzed the focal length, the spherical aberration, the chromatic aberration, and the effects of spontaneous emission on the spot size. Their approach was a wave-optical one, in which the atomic propagation was treated by considering the phase change of a de Broglie wave front as it passes through the lens. Diffraction of the atoms was thus included inherently in their approach. They found that, for reasonable laser and atomic-beam parameters, spot sizes of a fraction of a nanometer could be obtained.

Recently Gallatin and Gould[6] (GG) extended the wave-optical approach of Balykin and Letokhov to treat the lens

0740-3224/91/091974-13$05.00

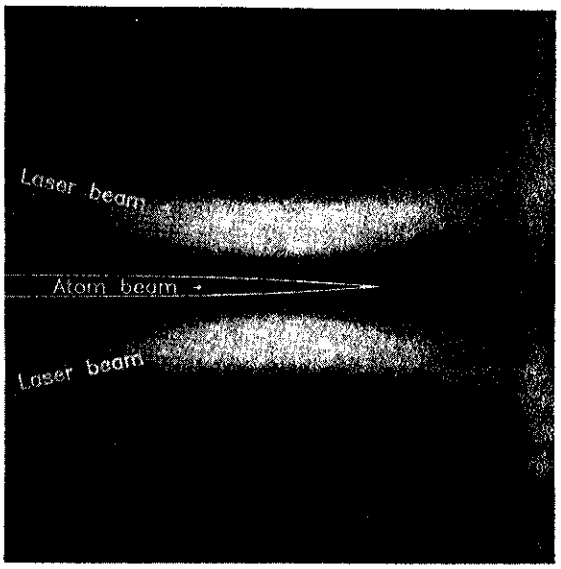

Fig. 1. Laser focusing of atoms in a TEM_{01}* laser beam. Cross-sectional view of the focus of the laser beam, with laser intensity represented by a gray scale. The atomic beam propagates coaxially with the laser beam, being focused by the gradient in the laser intensity.

correctly as a thick lens. They used a path integral formalism to solve Schrödinger's equation for the propagation of a Gaussian atomic beam in the TEM_{01}* laser field, obtaining focal spot sizes and positions of optimum focus for a number of realistic cases. They also estimated, in the thin-lens limit, the effects of spherical aberration, chromatic aberration, spontaneous emission, and dipole fluctuations. They found that, unlike for the result of Balykin and Letokhov, spherical aberration does not vanish for a particular set of laser-beam parameters. Further, they found the largest contributions to the spot size to be diffraction, spherical aberration, and dipole fluctuations. Spot sizes of several nanometers were calculated for the cases they examined.

Our approach to the analysis of the TEM_{01}* laser atomic lens is to treat the atoms as classical particles that are moving in the potential generated by the dipole force. We use methods that were originally developed for charged-particle optics for calculating the trajectories of particles in cylindrically symmetric potential fields. Applied to the TEM_{01}* laser atomic lens, these methods result in a simple understanding of the first-order focal properties. In fact the first-order paraxial equation is of exactly the same form as the equation solved by Glaser[7] for electron trajectories in a bell-shaped magnetic electron-microscope lens field. A simple solution exists, which treats the thickness of the lens exactly and predicts focal lengths and principal plane locations for both the immersion case (when the image or object is within the field of the lens) and the asymptotic case. The immersion case is particularly interesting for the TEM_{01}* laser atomic lens, because this is where the shortest focal lengths and hence the smallest aberrations occur. As is discussed in Section 2, we find that the lens has a minimum focal length (MFL), which is reached when the focal spot is at the center of the lens and the focal length is equal to the Rayleigh length of the laser beam. This has important design consequences in that infinitely short focal lengths cannot be achieved. In addition, the optimum configuration for obtaining the minimum spot size (in the zero-magnification case) is a symmetric arrangement with the focus at the center of the lens.

With analytic expressions for the first-order properties of the lens accurate expressions for contributions to the spot size can be obtained. Aberrations can be treated exactly without resorting to a thin-lens approximation. We obtain analytic expressions for spherical and chromatic aberration as well as compact expressions for the aberrations arising from both spontaneous emission and dipole-force fluctuations. Diffraction of the atoms is treated as it would be in the case of geometric optics; i.e., Fraunhofer diffraction of the atom beam is assumed, based on the de Broglie wavelength of the atoms and the angle of convergence of the beam at the focal spot. This assumption is valid provided that the potential does not change rapidly over the scale of an atomic wavelength, which is essentially the requirement for the WKB approximation. The effect on the spot diameter of a finite source size or, equivalently, an imperfectly collimated atomic beam is also simply obtained when the focal length and principal plane location are known.

In Section 2 we discuss the solution of the first-order paraxial equation of motion for the atoms in the TEM_{01}* laser field and discuss the resulting description of the lens in terms of cardinal elements. Section 3 covers spot size contributions. In Section 4 we discuss numerical examples, comparing our results with those of GG and examining the case of optimum focusing with the shortest focal length. Optimization of the lens is covered in Section 5, where a practical formula for the net spot size is derived and minimized.

2. FIRST-ORDER LENS PROPERTIES

A. Paraxial Equation of Motion

In this section we derive the first-order equation of motion that governs the focusing of a cylindrically symmetric atomic beam in the TEM_{01}* laser field. The optic axis, the axis of symmetry, is the z axis, with $z = 0$ located at the center of the laser focus (minimum beam waist). The equation of motion can be derived from the Lagrangian, $L = (\dot{x}^2 + \dot{y}^2 + \dot{z}^2)/2m - U(r, z)$, in the standard way.[8] Here $\dot{x}$ denotes the atomic velocity along the x axis, m is the atomic mass, and $U(r, z)$ is the potential energy. In cylindrical coordinates, assuming that the initial angular momentum about the z axis is zero, the radial equation of motion simplifies to

$$\ddot{r} + \frac{1}{m}\frac{\partial U(r,z)}{\partial r} = 0. \tag{1}$$

The conservation of energy is used to parameterize this equation in terms of the distance along the optic axis z. With this parameterization the all-orders equation of motion becomes

$$\frac{d}{dz}\left[\left(1 - \frac{U(r,z)}{E_0}\right)^{1/2}(1 + r'^2)^{-1/2}r'\right] + \frac{1}{2E_0}\left[1 - \frac{U(r,z)}{E_0}\right]^{-1/2}(1 + r'^2)^{1/2}\frac{\partial U(r,z)}{\partial r} = 0. \tag{2}$$

Here E_0 is the incident atomic-beam kinetic energy and r' denotes the differentiation of r with respect to z.

In order to solve Eq. (2), we need the potential energy $U(r,z)$ of the atom in the laser field. The potential energy is given by[4]

$$U(r,z) = \frac{\hbar\Delta}{2}\ln[1 + p(r,z)], \tag{3}$$

where $\Delta = \omega - \omega_0$ is the laser detuning from the atomic resonant frequency. Here ω and ω_0 are the laser and atomic resonance angular frequencies, and $p(r,z)$, the atomic transition saturation parameter, is given by

$$p(r,z) = \frac{I(r,z)}{I_s}\frac{\gamma^2}{\gamma^2 + 4\Delta^2}. \tag{4}$$

In the expression for $p(r,z)$, γ is the natural atomic resonance linewidth (in radians per second), I_s is the atomic saturation transition intensity, and $I(r,z)$ is the laser intensity distribution for the TEM_{01}* mode, given by

$$I(r,z) = 8I_0\frac{w_0^2 r^2}{w^4(z)}\exp\left(-\frac{2L^2}{w_0^2}\frac{r^2}{L^2 + z^2}\right). \tag{5}$$

The parameter w_0 determines the radius of the laser beam at the waist; the peak intensity is found at a distance $w_0/2^{1/2}$ from the axis. The quantity L is the Rayleigh length, given by $L = \pi w_0^2/\lambda$; λ is the laser wavelength; $w^2(z) = w_0^2(1 + z^2/L^2)$; and I_0 is the laser intensity at the beam waist, which is related to the laser power P_0 by $I_0 = P_0/2\pi w_0^2$.

The first-order solution of Eq. (2) involves making the assumptions that $U(r,z) \ll E_0$ and $r' \ll 1$. The equation then simplifies to

$$r'' + \frac{1}{2E_0}\frac{\partial U(r,z)}{\partial r} = 0. \tag{6}$$

We then expand the potential in r around the z axis. This expansion involves both the exponential in the expression for the laser-beam intensity and the logarithm in the expression for the potential. In order for this to be a valid expansion we require that $r^2 \ll w_0^2$ and $p(r,z) \ll 1$. When we take into account the first of these requirements, the second becomes $p_0 = \mathcal{O}(1)$, where p_0 is the space-independent part of $p(r,z)$:

$$p_0 = 8\frac{\gamma^2}{\gamma^2 + 4\Delta^2}\frac{I_0}{I_s}. \tag{7}$$

Expanding the potential, we find that the lowest-order term is quadratic in r:

$$U_2(r,z) = \frac{\hbar\Delta p_0 w_0^2}{2w^4(z)}r^2. \tag{8}$$

We note, as was pointed out by Balykin and Letokhov,[5] that this quadratic dependence on r provides the necessary radial dependence of the potential for a Newtonian lens description. Inserting Eq. (8) into Eq. (6) results in the first-order paraxial equation of motion:

$$r'' + p_0\frac{\hbar\Delta}{2E_0}\frac{w_0^2}{w^4(z)}r = 0. \tag{9}$$

At this point we introduce the excitation parameters k and q and rewrite the equation of motion in a dimensionless form. The excitation parameters are

$$k^2 = p_0\frac{\hbar\Delta}{2E_0}\frac{L^2}{w_0^2}, \tag{10}$$

$$q^2 = k^2 + 1. \tag{11}$$

The dimensionless variables are $R = r/L$ and $Z = z/L$. With these substitutions the first-order equation of motion, Eq. (9), can be written in the simple dimensionless form

$$R'' + \frac{k^2}{(1 + Z^2)^2}R = 0. \tag{12}$$

This differential equation can be cast in a form for which there is an analytic solution (first developed by Glaser[7]) by making the substitution $Z = -\cot\phi$. We note that $\phi = 0$ at $z = -\infty$ and $\phi = \pi$ at $z = +\infty$ (see Fig. 2). With this substitution the equation of motion becomes

$$R'' + 2\cot\phi R' + k^2R = 0 \tag{13}$$

(primes now indicate differentiation with respect to ϕ). A further substitution of $R(\phi) = y(\phi)/\sin\phi$ results in the simple differential equation

$$y'' + q^2y = 0. \tag{14}$$

The general solution to Eq. (14) is a linear combination of $\sin q\phi$ and $\cos q\phi$, which can be converted into a general expression for the dimensionless trajectory:

$$R(\phi) = (1/\sin\phi)(c_1\sin q\phi + c_2\cos q\phi), \tag{15}$$

where c_1 and c_2 are constants chosen to specify the trajectory of interest. For example, a ray moving in the positive z direction that is initially parallel to the z axis at a distance r_0 is described by the trajectory

$$R(\phi) = \frac{r_0}{L}\frac{\sin q\phi}{q\sin\phi}. \tag{16}$$

This trajectory is particularly useful in determining the cardinal elements of the lens; an example is shown in Fig. 2.

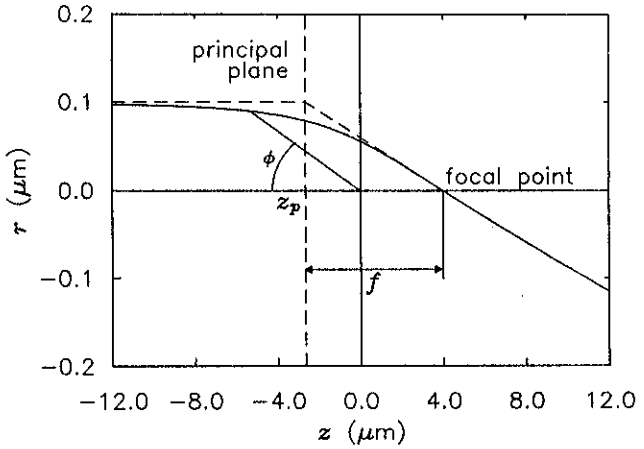

Fig. 2. Sample trajectory, described by Eq. (16), of an atom initially traveling parallel to the z axis at a radius of 0.1 μm. The locations of the focal point and the principal plane are shown along with the definitions of the angle ϕ and the focal length f. For this trajectory $q = 1.42$.

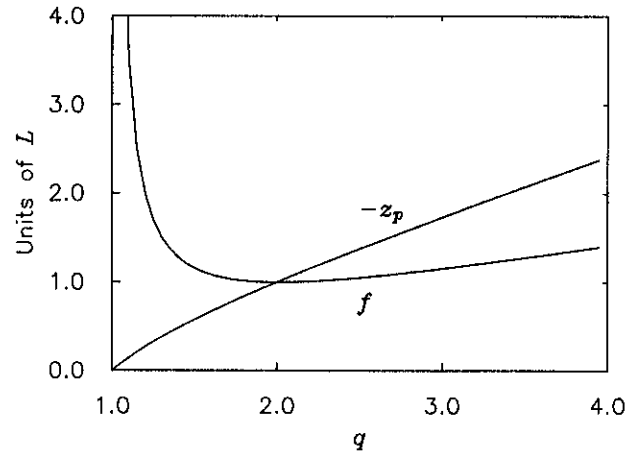

Fig. 3. Focal length f and principal plane location z_p as a function of q. Note that the focal length has a minimum at $q = 2$, where $z_p = -f$.

B. Cardinal Elements

Since the first-order paraxial equation for the TEM_{01}* laser atomic lens is identical to the equation treated by Glaser in his bell-shaped magnetic lens field model, we can extract all the first-order properties of the lens from his work. The lens has the following important characteristics: (a) It is a thick lens, and hence its cardinal elements include both principal planes and focal lengths instead of only a single focal length. (b) It is a symmetric lens, so the principal planes and the focal spots for the image side and object side are located at equal distances from the lens center. (c) For sufficiently large excitation, the lens can have multiple crossovers. (d) For all image and object plane locations, even in the immersion case, the lens is still Newtonian in the sense that the simple Newtonian lens law applies for determining magnification, image locations, etc. in terms of the cardinal elements of the lens.

We determine the image-side focal point of the lens by considering the initially parallel trajectory described by Eq. (16). A focal point exists for the values of ϕ ($0 < \phi < \pi$) that result in $R(\phi) = 0$. This occurs when $\phi = n\pi/q$, where n is an integer between 1 and the largest integer less than q. Thus the image-side focal points are given by

$$z_f = L \cot(n\pi/q). \tag{17}$$

We see that for $1 \le q \le 2$ the lens has a single focal point that ranges in location from $z = +\infty$ to $z = 0$. The principal plane locations and focal lengths are determined from the trajectory of Eq. (16), as shown in Fig. 2. Using Eq. (16), we obtain the image-side principal plane locations,

$$\begin{aligned} z_p &= -L \cot(n\pi/2q) \qquad (n \text{ odd}), \\ z_p &= L \tan(n\pi/2q) \qquad (n \text{ even}), \end{aligned} \tag{18}$$

and the focal lengths,

$$f = (-1)^{n+1} \frac{L}{\sin(n\pi/q)}. \tag{19}$$

The linear and angular magnifications, M and m, are given by

$$M = \frac{1}{m} = (-1)^n \frac{\sin \phi_o}{\sin \phi_i}, \tag{20}$$

where ϕ_o and ϕ_i are the values of ϕ that correspond to the object and image positions, respectively. We note that, though it is not required for treatment in terms of cardinal elements, the lens behavior is simplest when the number of focal points is kept to one. Hence Eqs. (17)–(20) are generally used with $n = 1$.

Figure 3 shows the behavior of the focal length f and the principal plane location z_p as a function of lens excitation q. Several interesting features of the lens become apparent on examination of these curves. For example, all the first-order properties of the lens are determined by a single parameter q, which is given by Eqs. (10)–(11). This fact makes characterization of the lens simple and shows that, at least to first order, there are many combinations of incident atomic velocity, laser power, detuning, and laser-beam waist w_0 that result in identical lens behaviors.

Furthermore, as is shown in Fig. 3, the focal length goes through a minimum, which is reached when $q = 2$. Thus the focusing of the lens does not become infinitely strong as the excitation is increased, as might have been expected. Instead, for $q > 2$, as a function of excitation the principal plane moves in the negative z direction faster than does the focal point, resulting in a longer focal length. The shortest focal length occurs when $f = L$ and $z_p = -L$; i.e., the focal point is at the center of the lens. This is sometimes referred to as the telescopic mode of focusing, because the trajectory enters and leaves the lens parallel to the z axis. The minimum focal length condition has important implications when the optimization of the lens is considered, as this is generally a configuration in which diffraction and some aberrations are minimized.

3. SPOT SIZE LIMITATIONS

The determination of the spot size for an initially (nearly) parallel atomic beam that is brought to a focus at the focal point of the lens is of central importance in the analysis of the TEM_{01}* laser atomic lens. We consider the contributions of aberrations as well as the effects of diffraction and a finite source size (i.e., an imperfectly collimated atomic beam). The aberrations include spherical aberration, chromatic aberration, and two diffusive aberrations, one resulting from spontaneous emission and the other from dipole-force fluctuations. In each case the ultimate result is an expression for the FWHM spot diameter of the beam at the focus in terms of laser- and atomic-beam parameters. To obtain the net spot size, we add all contributions in quadrature.

A. Aberrations

Because of the simple analytic nature of the paraxial solutions to the ray equation, it is possible to do a fairly rigorous treatment of the aberrations. Though the immediate interest is in the spot size at the focus for an initially parallel beam, we obtain expressions for the aberrations in the general case of finite object and image distances. These will prove useful in cases in which the lens is used for imaging. We then consider the limiting case of zero magnification (i.e., the object at $-\infty$, the image at the

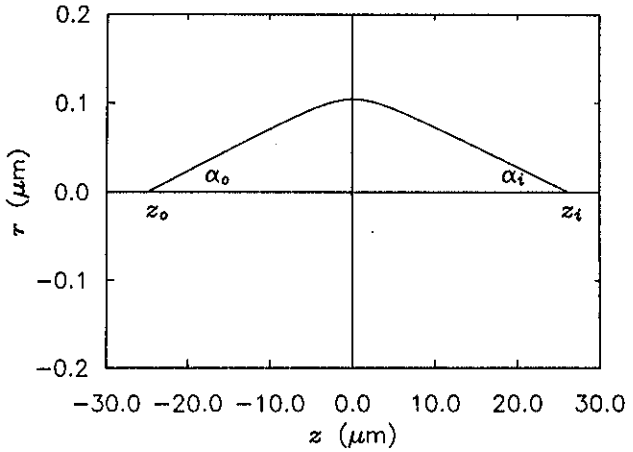

Fig. 4. Trajectory $R_1(Z)$ used in determining aberration coefficients for finite object and image distances. The ray crosses the z axis at the object position z_o with slope α_o and again at the image position z_i with slope α_i. For this particular ray $\alpha_o = 0.025$, $q = 1.15$, and $L = 5.33$ μm.

focal point) and obtain expressions for the FWHM spot diameters.

All the aberrations of the lens are treated with essentially the same method, in which a (small) deviation ε from the paraxial trajectory is calculated. The method is described in several texts on electron optics.[9-11] For each aberration we arrive at a differential equation for the deviation ε that is the same as the paraxial equation [Eq. (12)] with an additional inhomogeneous term on the right-hand side. This inhomogeneous differential equation is solved by the method of variation of parameters.[12] The method involves choosing two linearly independent solutions to Eq. (12), $R_1(Z)$ and $R_2(Z)$. If we choose $R_1(Z)$ such that it equals zero at the image plane ($Z = Z_i$), the deviation in R_1 at the image plane caused by an aberration can be expressed in terms of the following integral (see, e.g., Ref. 9):

$$\varepsilon = \frac{R_2(Z_i)}{R_1R_2' - R_1'R_2}\int_{Z_o}^{Z_i} R_1(Z)W(R_1, R_1', Z)\mathrm{d}Z, \tag{21}$$

where $W(R_1, R_1', Z)$ is the inhomogeneous term in the differential equation. The quantity $R_1R_2' - R_1'R_2$ is the Wronskian of the two solutions R_1 and R_2, which is a constant because of their linear independence.

In the general case, when the object and image planes are both at finite distances from the lens, it is most useful to define aberration coefficients, which are used for determining the trajectory error at the image plane for a trajectory R_1 that originates on the axis at the object with a slope α_o. This trajectory, shown in Fig. 4, also crosses the axis at the image plane, making an angle $\alpha_i = \alpha_o/|M|$, where M is the linear magnification of the lens. Following electron-optical conventions, we define spherical-, chromatic-, spontaneous-emission-, and dipole-fluctuation-aberration coefficients C_{sph}^o, C_{chr}^o, C_{spont}^o, and C_{dip}^o, referenced to the object plane, by the following relations:

$$|\varepsilon_{sph}| = |M|\alpha_o^3(C_{sph}^o/L), \tag{22}$$

$$|\varepsilon_{chr}| = |M|\alpha_o\epsilon(C_{chr}^o/L), \tag{23}$$

$$|\varepsilon_{spont}| = |M|\alpha_o(C_{spont}^o/L), \tag{24}$$

$$|\varepsilon_{dip}| = |M|\alpha_o^3(C_{dip}^o/L), \tag{25}$$

where ϵ is a fractional deviation in the energy of the atom beam, to be discussed below. Absolute values of ε and M are taken so that the aberration coefficients can be related to spot diameters. The powers of α_o used in these definitions are chosen in order to remove any α_o dependence from the coefficients themselves. That the correct power has been chosen for each aberration will become clear below. Since the spontaneous and dipole aberrations are diffusive in nature, the quantities ε_{spont} and ε_{dip} are interpreted as rms values.

To determine the aberration coefficients, we require an explicit expression for the ray R_1. For convenience we characterize the trajectories in terms of the variable $\phi = \arctan Z + \pi/2$ instead of in terms of Z and use solutions of the form shown in Eq. (15). We write $R_1(\phi) = \alpha_o h(\phi)$, where

$$h(\phi) = \frac{\sin[q(\phi - \phi_o)]}{q\sin\phi\sin\phi_o}. \tag{26}$$

For R_2 we choose an independent solution that has the property $R_2(\phi_o) = 1$, so that at the image plane $R_2(\phi_i) = M$. Although we do not need the explicit form of R_2, we note that it is

$$R_2(\phi) = g(\phi) = \frac{\sin\phi_o}{\sin\phi}\frac{\sin[q(\phi - \alpha)]}{\sin[q(\phi_o - \alpha)]}, \tag{27}$$

where $\alpha = \phi_o - (1/q)\tan^{-1}(q\tan\phi_o)$. The trajectories $h(\phi)$ and $g(\phi)$ are the standard trajectories used for aberration analysis in electron optics.[10]

With this choice of R_1 and R_2 the denominator in Eq. (21) becomes $-\alpha_o$, and we can write

$$\varepsilon = -M\int_{\phi_o}^{\phi_i} h(\phi)W(\alpha_o h, \alpha_o h', \phi)\frac{\mathrm{d}Z}{\mathrm{d}\phi}\mathrm{d}\phi. \tag{28}$$

Using Eqs. (22) and (23), we can now write

$$C_{sph}^o = \left|\frac{L}{\alpha_o^3}\int_{\phi_o}^{\phi_i} h(\phi)W_{sph}(\alpha_o h, \alpha_o h', \phi)\frac{\mathrm{d}\phi}{\sin^2\phi}\right| \tag{29}$$

$$C_{chr}^o = \left|\frac{L}{\alpha_o\epsilon}\int_{\phi_o}^{\phi_i} h(\phi)W_{chr}(\alpha_o h, \alpha_o h', \phi)\frac{\mathrm{d}\phi}{\sin^2\phi}\right|. \tag{30}$$

The expressions for the diffusive-aberration coefficients C_{spont}^o and C_{dip}^o are similar to Eqs. (29) and (30), though a little more complicated because of the random nature of the forces involved. They will be discussed in more detail below.

Determining the aberration coefficients is now reduced to finding the inhomogeneous terms for each aberration source and carrying out the integrations in Eqs. (29) and (30).

1. *Spherical Aberration*

Spherical aberration arises when higher-order terms in the expansion of the equation of motion are not neglected. This is a manifestation of the fact that for large enough r the potential is no longer simply quadratic in r. Since the

potential is cylindrically symmetric, the next-higher term is proportional to r^4. The equation of motion depends on $\partial U/\partial r$, so its next-higher term is of the order of r^3. To include all terms in r^3 correctly, we must keep contributions from the expansion of the all-orders equation of motion [Eq. (2)] as well as contributions from the expansion of the potential. The resulting third-order inhomogeneous term is

$$W_{\text{sph}}(R,R',Z) = k^2R^3\left[\left(p_0\frac{L^2}{w_0^2}-k^2\right)\frac{1}{(1+Z^2)^4} + 4\frac{L^2}{w_0^2}\frac{1}{(1+Z^2)^3}\right] - k^2R^2R'\left[\frac{2Z}{(1+Z^2)^3}\right] - k^2RR'^2\left[\frac{1}{(1+Z^2)^2}\right]. \tag{31}$$

Converting Z to ϕ and R to $\alpha_o h(\phi)$, we can insert Eq. (31) into Eq. (29) to obtain an explicit integral for the spherical aberration coefficient:

$$\begin{aligned} C_{\text{sph}}{}^o = \Bigg| & \frac{k^2L}{q^4\sin^4\phi_o}\left(p_0\frac{L^2}{w_0^2}+4\right) \times \int_{\phi_o}^{\phi_i}\sin^2\phi\,\sin^4[q(\phi-\phi_o)]\,d\phi \\ & + \frac{k^2L}{q^4\sin^4\phi_o}\left(4\frac{L^2}{w_0^2}-3\right) \times \int_{\phi_o}^{\phi_i}\sin^4[q(\phi-\phi_o)]\,d\phi \\ & - \frac{k^2L}{q^2\sin^4\phi_o} \times \int_{\phi_o}^{\phi_i}\sin^2\phi\,\sin^2[q(\phi-\phi_o)]\,d\phi \\ & + \frac{4k^2L}{q^3\sin^4\phi_o} \times \int_{\phi_o}^{\phi_i}\sin\phi\cos\phi\cos[q(\phi-\phi_o)] \\ & \times \sin^3[q(\phi-\phi_o)]\,d\phi\Bigg|. \end{aligned} \tag{33}$$

All the integrals in Eq. (33) can be done analytically, and the resulting spherical-aberration coefficient, referenced to the object plane, is given by

$$\begin{aligned} C_{\text{sph}}{}^o = & \frac{L}{\sin^4\phi_o}\frac{3\pi k^2}{8q^5}\left[\frac{L^2}{2w_0^2}(p_0+8)-\frac{5+2k^2}{3}\right] \\ & - \frac{L}{\sin^4\phi_o}\frac{1}{8(4k^2+3)}\left(3p_0\frac{L^2}{w_0^2}+15-4k^2\right) \\ & \times\left[\sin\left(2\phi_o+\frac{2\pi}{q}\right)-\sin(2\phi_o)\right]. \end{aligned} \tag{34}$$

In going from Eq. (33) to Eq. (34), we have used the object–image relation

$$\phi_i = \phi_o + (n\pi/q), \tag{35}$$

obtained from finding the zeros of $h(\phi)$. In addition, we have restricted ourselves to the case in which $n = 1$, so Eq. (34) is valid only for the first image in a multiple-crossover lens. The absolute value has been dropped because the sign of $C_{\text{sph}}{}^o$ can be shown to remain unchanged for all excitations.[9]

The spherical-aberration coefficient given in Eq. (34) can be used in this form for any situation in which the object and image positions are finite. However, it is often convenient to expand the coefficient as a polynomial in $1/M$. This is useful if the main design consideration of a lens is the magnification or if M is particularly large or small. It can be shown[10,11] that $C_{\text{sph}}{}^o$ can be uniquely represented by a fourth-order polynomial, i.e.,

$$C_{\text{sph}}{}^o = C_{\text{sph0}}{}^o + \frac{C_{\text{sph1}}{}^o}{M} + \frac{C_{\text{sph2}}{}^o}{M^2} + \frac{C_{\text{sph3}}{}^o}{M^3} + \frac{C_{\text{sph4}}{}^o}{M^4}. \tag{36}$$

The coefficients of the polynomial can be extracted from Eq. (34) by means of the relationship

$$-\cot\phi_o = \frac{1}{M\sin(\pi/q)} + \cot(\pi/q), \tag{37}$$

which is derived from the expressions for the magnification, Eq. (20), and the object–image relation, Eq. (35). Substituting Eq. (37) into Eq. (34), we get the polynomial coefficients

$$\begin{aligned} C_{\text{sph0}}{}^o = C_{\text{sph4}}{}^o = & \frac{3\pi k^2L}{8q^5\sin^4(\pi/q)}\left[\frac{L^2}{2w_0^2}(p_0+8)-\frac{5+2k^2}{3}\right] \\ & - \frac{L\sin(2\pi/q)}{8(4k^2+3)\sin^4(\pi/q)}\left(3p_0\frac{L^2}{w_0^2}+15-4k^2\right), \end{aligned} \tag{38}$$

$$\begin{aligned} C_{\text{sph1}}{}^o = & C_{\text{sph3}}{}^o \\ = & \frac{3\pi k^2L\cos(\pi/q)}{2q^5\sin^4(\pi/q)}\left[\frac{L^2}{2w_o^2}(p_0+8)-\frac{5+2k^2}{3}\right] \\ & - \frac{L[3+\cos(2\pi/q)]}{4(4k^2+3)\sin^3(\pi/q)}\left(3p_0\frac{L^2}{w_0^2}+15-4k^2\right), \end{aligned} \tag{39}$$

$$\begin{aligned} C_{\text{sph2}}{}^o = & \frac{3\pi k^2L[2+\cos(2\pi/q)]}{4q^5\sin^4(\pi/q)}\left[\frac{L^2}{2w_0^2}(p_0+8)-\frac{5+2k^2}{3}\right] \\ & - \frac{3L\cos(\pi/q)}{2(4k^2+3)\sin^3(\pi/q)}\left[3p_0\frac{L^2}{w_0^2}+15-4k^2\right]. \end{aligned} \tag{40}$$

The expression for $C_{\text{sph}}{}^o$ in terms of M is useful for most imaging situations because the coefficients need be calculated only once and the spherical aberration is known for all object–image distances. However, it poses a slight problem when we wish to consider the zero-magnification (parallel-in) case because $C_{\text{sph}}{}^o$ becomes infinite while α_o goes to zero. The spot size, of course, does not become infinite. The way around this awkwardness is to use the spherical-aberration coefficient $C_{\text{sph}}{}^i$ that is defined in terms of the trajectory angle α_i at the image plane. We write

$$|\varepsilon_{\mathrm{sph}}| = \alpha_i{}^3 \frac{C_{\mathrm{sph}}{}^i}{L}, \tag{41}$$

which then requires that

$$C_{\mathrm{sph}}{}^i = M^4 C_{\mathrm{sph}}{}^o, \tag{42}$$

where we have used the fact that $\alpha_i = \alpha_o/|M|$. Using Eqs. (42) and (36), we find that

$$C_{\mathrm{sph}}{}^i(M = 0) = C_{\mathrm{sph4}}{}^o. \tag{43}$$

Equation (41) can now be used to obtain the spot size for the zero-magnification case. To obtain the minimum spot size, we note that the diameter can be taken at the circle of least confusion, at which point the FWHM spot size δ_{sph} is given by $\frac{1}{2}L|\varepsilon_{\mathrm{sph}}|$. For a ray that is incident at a radius r_0, the angle at the image plane is given by

$$\alpha_i = \frac{r_0}{f} = \frac{r_0}{L}\sin(\pi/q). \tag{44}$$

The final expression for the spot size arising from spherical aberration at the circle of least confusion then becomes

$$\delta_{\mathrm{sph}} = \frac{3\pi k^2 r_0{}^3}{16L^2q^5\sin(\pi/q)}\left[\frac{L^2}{2w_0{}^2}(p_0 + 8) - \frac{5 + 2k^2}{3}\right] - \frac{r_0{}^3\cos(\pi/q)}{8L^2(4k^2 + 3)}\left(3p_0\frac{L^2}{w_0{}^2} + 15 - 4k^2\right). \tag{45}$$

2. Chromatic Aberration

Chromatic aberration arises from a finite energy spread in the incident atomic beam. Atoms with different initial kinetic energies follow different trajectories through the lens, resulting in a smearing of the focal spot.

The chromatic-aberration coefficient can be calculated in a way analogous to the method for the spherical aberration. The energy E_0 in the paraxial equation (9) must be replaced by $E_0(1 + \epsilon)$, where ϵ is a fractional energy deviation. When the equation is expanded and the lowest-order terms retained, the following differential equation results:

$$r'' + \frac{\hbar\Delta p_0}{2E_0}\frac{w_0{}^2}{w^4(z)}r = \epsilon\frac{\hbar\Delta p_0}{2E_0}\frac{w_0{}^2}{w^4(z)}r. \tag{46}$$

We see that the inhomogeneous term in this case is

$$W_{\mathrm{chr}}(R, R', Z) = \frac{k^2}{(1 + Z^2)^2}\epsilon R, \tag{47}$$

where the conversion to dimensionless variables has been carried out. Substituting Eq. (47) into Eq. (30) and using the object–image relation, Eq. (35), yields the chromatic-aberration coefficient

$$C_{\mathrm{chr}}{}^o = \frac{\pi k^2 L}{2q^3\sin^2\phi_o}. \tag{48}$$

Equation (48) is an exact expression for the chromatic-aberration coefficient in the finite object–image case. As with spherical aberration, it is useful to write it in terms of a polynomial in the linear magnification M. In this case it is necessary to include only powers up to M^{-2}:

$$C_{\mathrm{chr}}{}^o = C_{\mathrm{chr0}}{}^o + \frac{C_{\mathrm{chr1}}{}^o}{M} + \frac{C_{\mathrm{chr2}}{}^o}{M^2}. \tag{49}$$

The expansion coefficients are given by

$$C_{\mathrm{chr0}}{}^o = C_{\mathrm{chr2}}{}^o = -\frac{\pi k^2 L}{2q^3}\frac{1}{\sin^2(\pi/q)}, \tag{50}$$

$$C_{\mathrm{chr1}}{}^o = -\frac{\pi k^2 L}{q^3}\frac{\cos(\pi/q)}{\sin^2(\pi/q)}. \tag{51}$$

Converting to the image-plane chromatic-aberration coefficient, defined by

$$|\varepsilon_{\mathrm{chr}}| = \alpha_i\epsilon(C_{\mathrm{chr}}{}^i/L), \tag{52}$$

we obtain

$$C_{\mathrm{chr}}{}^i = M^2 C_{\mathrm{chr}}{}^o, \tag{53}$$

from which we arrive at the FWHM spot diameter for the zero-magnification case:

$$\delta_{\mathrm{chr}} = \frac{\pi k^2 r_0}{2q^3\sin(\pi/q)}\frac{\Delta E_{1/2}}{E_0}, \tag{54}$$

where $\Delta E_{1/2}$ is the FWHM of the energy distribution of the atomic beam.

3. Diffusive Aberrations

Since the spontaneous and dipole aberrations are the result of random forces, the average deviation along a particle trajectory is zero. The deviations from the paraxial trajectories must therefore be treated in terms of rms values. The formalism for this calculation resembles the treatment of Brownian motion.[13] We consider the radial equation of motion, Eq. (1), with an additional inhomogeneous force term on the right-hand side:

$$\ddot{r} + \frac{1}{m}\frac{\partial U(r, z)}{\partial r} = \frac{1}{m}F_r(t). \tag{55}$$

$F_r(t)$ is a random force for which $\langle F_r(t)\rangle = 0$ but $\langle F_r(t)F_r(t')\rangle \neq 0$. Converting Eq. (55) to a paraxial form, we make the approximation $z \approx v_0 t$, where $v_0 = (2E_0/m)^{1/2}$ is the initial atomic velocity, and write

$$r'' + \frac{1}{2E_0}\frac{\partial U(r, z)}{\partial r} = \frac{1}{2E_0}F_r\left(\frac{z}{v_0}\right). \tag{56}$$

Converting to dimensionless variables, we can make the association

$$W(R, R', Z) = \frac{L}{2E_0}F_r\left(\frac{LZ}{v_0}\right). \tag{57}$$

This step allows us to write an expression for the mean-square trajectory deviation that is similar to Eq. (21), though it contains a double integral to account for the random nature of W. To simplify the following expressions, we suppress the explicit R and R' dependence in W, writing only $W(Z)$ and bearing in mind that some of the Z dependence may come through an R or R' dependence. We get

$$\langle\varepsilon^2\rangle = \frac{R_2(Z_i)^2}{(R_1R_2' - R_1'R_2)^2}\int_{Z_o}^{Z_i}\mathrm{d}Z\int_{Z_o}^{Z_i}\mathrm{d}Z' R_1(Z)R_1(Z') \times \langle W(Z)W(Z')\rangle. \tag{58}$$

Putting, as before, the solution $R_1 = \alpha_o h(\phi)$ into Eq. (58) and changing variables from Z to ϕ, we obtain expressions for the spontaneous- and dipole-aberration coefficients:

$$C_{\text{spont}}{}^{o} = \frac{L}{\alpha_o}\left[\int_{\phi_o}^{\phi_i}\frac{d\phi}{\sin^2\phi}\int_{\phi_o}^{\phi_i}\frac{d\phi'}{\sin^2\phi'}h(\phi)h(\phi')\times\langle W_{\text{spont}}(\phi)W_{\text{spont}}(\phi')\rangle\right]^{1/2}, \tag{59}$$

$$C_{\text{dip}}{}^{o} = \frac{L}{\alpha_o{}^3}\left[\int_{\phi_o}^{\phi_i}\frac{d\phi}{\sin^2\phi}\int_{\phi_o}^{\phi_i}\frac{d\phi'}{\sin^2\phi'}h(\phi)h(\phi')\times\langle W_{\text{dip}}(\phi)W_{\text{dip}}(\phi')\rangle\right]^{1/2}. \tag{60}$$

In order to use Eqs. (59) and (60), we must now determine the autocorrelations of the inhomogeneous terms W_{spont} and W_{dip}.

The spontaneous-emission aberration arises as a result of the random momentum changes of size h/λ, which occur each time a photon is spontaneously emitted. The average rate at which these changes occur depends on the intensity of the laser, and for low intensities it equals $\gamma p/2$, where γ is the natural linewidth of the atomic transition in radians per second and p is the saturation parameter given in Eq. (4).[4] Over the time scale of interest, i.e., the time over which the focusing potential changes as the atom passes through the lens, the momentum changes can be considered to occur over an infinitely short time and to be completely uncorrelated. With this assumption we can write

$$\langle F_{\text{spont}}(t)F_{\text{spont}}(t')\rangle = \frac{2}{3}\gamma\frac{p(r,z)}{2}\left(\frac{h}{\lambda}\right)^2\delta(t-t'). \tag{61}$$

The factor of 2/3 is a result of averaging over two of the three spatial degrees of freedom in the spontaneous-emission process. Assuming paraxial conditions, we can write the saturation parameter $p(r,z)$ in terms of ϕ as

$$p(r,z) \approx p_0\frac{L^2}{w_0{}^2}\frac{R^2}{(1+Z^2)^2} = p_0\frac{L^2}{w_0{}^2}R^2(\phi)\sin^4\phi. \tag{62}$$

Combining Eqs. (57) and (61) and relation (62), we can deduce

$$\langle W_{\text{spont}}(\phi)W_{\text{spont}}(\phi')\rangle = \frac{L^3h^2v_0\gamma p_0}{12w_0{}^2E_0{}^2\lambda^2}R^2(\phi)(\sin^6\phi)\delta(\phi-\phi'), \tag{63}$$

where we have used the fact that $\delta(Z-Z') = \sin^2\phi\,\delta(\phi-\phi')$. Inserting Eq. (63) for the autocorrelation of the spontaneous-emission inhomogeneous term into the expression for the aberration coefficient [Eq. (59)] and substituting $R(\phi) = \alpha_o h(\phi)$, we obtain

$$C_{\text{spont}}{}^{o} = \frac{L^2h}{\lambda w_0E_0}\left[\frac{Lv_0\gamma p_0}{12}\int_{\phi_o}^{\phi_i}h^4(\phi)(\sin^2\phi)d\phi\right]^{1/2}. \tag{64}$$

Putting in the definition of $h(\phi)$ [Eq. (26)], we get

$$C_{\text{spont}}{}^{o} = \frac{L^2h}{\lambda w_0E_0}\left(\frac{Lv_0\gamma p_0}{12}\right)^{1/2}\frac{1}{q^2\sin^2\phi_o}\times\left[\int_{\phi_o}^{\phi_i}\frac{\sin^4[q(\phi-\phi_o)]}{\sin^2\phi}\right]^{1/2}. \tag{65}$$

The integral in Eq. (65) is not analytic, so a numerical evaluation of this equation must be used to obtain the aberration coefficient. In addition, a convenient expansion into a polynomial in the magnification is not possible. Nevertheless, the expression is still useful when one is interested in the aberration coefficient for the finite-magnification case.

Since the magnification expansion is not possible, and hence we cannot easily convert to the aberration coefficient referenced to the image plane, another approach must be taken to obtain the spot size for the zero-magnification case. Instead of letting $R_1 = \alpha_o h(\phi)$ in Eq. (58), we can use the parallel-in trajectory of Eq. (16), since the choice of solutions in the method of the variation of parameters is arbitrary. We note that this trajectory crosses the axis at the focus, so Eq. (58) is still valid. A linearly independent solution is needed for R_2, for which we use

$$R_2 = -\sin(\pi/q)\frac{\cos(q\phi)}{\sin\phi}. \tag{66}$$

We note that $R_2 = 1$ at the focus ($\phi = \pi/q$). The Wronskian of R_1 and R_2 is now $-(r_0/L)\sin(\pi/q)$, and we can write

$$\langle\varepsilon^2\rangle = \frac{L^2}{r_0{}^2\sin^2(\pi/q)}\int_0^{\pi/q}\frac{d\phi}{\sin^2\phi}\int_0^{\pi/q}\frac{d\phi'}{\sin^2\phi'}R_1(\phi)R_1(\phi')\times\langle W(\phi)W(\phi')\rangle. \tag{67}$$

Putting Eqs. (63) and (16) into this expression leads to an expression for the zero-magnification aberration coefficient referenced to the image plane (defined by $\varepsilon_{\text{spont}} = |\alpha_i|C_{\text{spont}}{}^{i}/L$):

$$C_{\text{spont}}{}^{i}(M=0) = \frac{L}{q^2\sin^2(\pi/q)}\left(\frac{L^3h^2v_0\gamma p_0}{12w_0{}^2E_0{}^2\lambda^2}\right)^{1/2}\times\left(\int_0^{\pi/q}\frac{\sin^4 q\phi}{\sin^2\phi}d\phi\right)^{1/2}, \tag{68}$$

where we have used the fact that $\alpha_i = r_0/f = r_0\sin(\pi/q)/L$. The FWHM spot diameter follows immediately from this result, i.e.,

$$\delta_{\text{spont}} = 2(2\ln 2)^{1/2}\frac{r_0}{q^2\sin(\pi/q)}\left(\frac{L^3h^2v_0\gamma p_0}{12w_0{}^2E_0{}^2\lambda^2}\right)^{1/2}\times\left(\int_0^{\pi/q}\frac{\sin^4 q\phi}{\sin^2\phi}d\phi\right)^{1/2}, \tag{69}$$

where the factor of $2(2\ln 2)^{1/2}$ provides the conversion from the rms to the FWHM.

The dipole fluctuation aberration is treated in a manner identical to the spontaneous-emission aberration. As was discussed by Dalibard and Cohen-Tannoudji,[14] the dipole force can reverse sign temporarily each time a photon is spontaneously emitted. The fluctuating part of the dipole force that results from this random sign change can be considered an inhomogeneous driving term $F_r(t)$ in the equation of motion, for which $\langle F_r(t)\rangle = 0$ but $\langle F_r(t)F_r(t')\rangle \neq 0$, just as with spontaneous emission. For small saturation parameters $p \ll 1$, the autocorrelation of the fluctuating part of the dipole force can be written as[14]

$$\langle F_{\text{dip}}(t)F_{\text{dip}}(t')\rangle = \frac{\hbar^2\Delta^2}{4}(\nabla p)^2p^2\exp(-\gamma|t-t'|). \tag{70}$$

Using the expression in relation (62) for the saturation parameter in the TEM_{01}^* laser atomic lens, letting $\nabla \rightarrow \partial/\partial r$, and converting t to LZ/v_0 as before, we can write

$$\langle W_{\mathrm{dip}}(Z)W_{\mathrm{dip}}(Z')\rangle = k^4 {p_0}^2 \frac{L^4}{{w_0}^4} \frac{R^6(Z)}{(1+Z^2)^8} \exp\left(-\frac{\gamma L}{v_0}|Z-Z'|\right). \tag{71}$$

This expression leads to a complicated integral when conversion is made to the variable ϕ for calculating the aberration coefficient. It suffices at present to consider the limit $\gamma L/v_0 \gg 1$, which occurs when the number of spontaneous emissions is large during transit through the lens. The approximation should be good because the aberration itself is significant only when a large number of spontaneous-emission events takes place. In this limit we can say that

$$\exp\left(-\frac{\gamma L}{v_0}|Z-Z'|\right) \approx \frac{2v_0}{\gamma L}\delta(Z-Z'). \tag{72}$$

We can now write an approximate autocorrelation in ϕ of the inhomogeneous term in the differential equation:

$$\langle W_{\mathrm{dip}}(\phi)W_{\mathrm{dip}}(\phi')\rangle = 2\frac{v_0}{\gamma L}k^4{p_0}^2\frac{L^4}{{w_0}^4}R^6(\phi)(\sin^{18}\phi)\delta(\phi-\phi'). \tag{73}$$

This equation can be inserted into Eq. (60) to yield the dipole-fluctuation-aberration coefficient:

$$C_{\mathrm{dip}}{}^o = \frac{L^3}{{\omega_0}^2}\left(\frac{2v_0}{\gamma L}\right)^{1/2}\frac{k^2p_0}{q^4\sin^4\phi_o} \times \left[\int_{\phi_o}^{\phi_i}\sin^6\phi\,\sin^8[q(\phi-\phi_o)]\mathrm{d}\phi\right]^{1/2}. \tag{74}$$

The integral in Eq. (74) is analytic but extremely cumbersome. Therefore, as with the spontaneous aberration, we do not perform the expansion in magnification but rather leave the expression for the aberration coefficient as it is for use in the finite-magnification case. For the zero-magnification case, we proceed as we did with the spontaneous aberration, making use of the parallel-in trajectory for R_1 in Eq. (58). Using Eq. (67) with Eq. (73) gives a zero-magnification aberration coefficient, referenced to the image plane, of

$$C_{\mathrm{dip}}{}^i(M=0) = \frac{L^3}{{w_0}^2}\left(\frac{2v_0}{\gamma L}\right)^{1/2}\frac{k^2p_0}{q^4\sin^4(\pi/q)} \times \left[\int_0^{\pi/q}\sin^6\phi(\sin^8 q\phi)\mathrm{d}\phi\right]^{1/2} \tag{75}$$

and a FWHM spot diameter of

$$\delta_{\mathrm{dip}} = 4(\ln 2)^{1/2}\frac{{r_0}^3}{{w_0}^2}\left(\frac{v_0}{\gamma L}\right)^{1/2}\frac{k^2p_0}{q^4\sin(\pi/q)} \times \left[\int_0^{\pi/q}\sin^6\phi(\sin^8 q\phi)\mathrm{d}\phi\right]^{1/2}. \tag{76}$$

B. Diffraction

The treatment of diffraction is straightforward once the paraxial trajectories are known. Since the potential in the lens is slowly varying as a function of z on the scale of the de Broglie wavelength λ_{dB} of the atom, we may apply the WKB approximation and make a complete analogy with the way diffraction is treated in ordinary geometric-light optics. For a given initial intensity distribution in the atomic beam the final spot size can be determined from knowledge of the trajectories in exactly the same manner as it would be for a light beam. For instance, a diffraction-limited Gaussian atomic beam with a given waist radius and location can be propagated through the lens with the ray transfer ($ABCD$) matrix derived from the principal plane locations and focal lengths. The spot size and location can be inferred from the radius of curvature and beam radius after the lens. Since the lens is Newtonian in the immersion case as well as in the asymptotic case, this approach is valid even when the focal spot is inside the lens.

Alternatively, one can assume that the atomic beam has a constant, circular intensity distribution formed by real apertures. In this case ordinary Fraunhofer diffraction is the appropriate optical analogy, and we obtain a simple expression for the FWHM of the diffracted intensity distribution at the image plane:

$$\delta_{\mathrm{diffr}} = \frac{0.61\lambda_{\mathrm{dB}}}{\alpha_i}. \tag{77}$$

For a beam that is initially parallel to the z axis with radius r_0, α_i is given by r_0/f, where f is the focal length of the lens. Thus the FWHM spot diameter at the focus is

$$\delta_{\mathrm{diffr}} = \frac{0.61\lambda_{\mathrm{dB}}L}{r_0\sin(\pi/q)}. \tag{78}$$

C. Finite Source Size

A perfectly parallel beam can be considered as arising from an infinitesimal source at $z=-\infty$. Of course, any real experiment has a finite source, or object, of size d_o and a finite object–distance z_o. This means that the focal spot will contain an image of the source, reduced in size by the magnification $M = z_i/z_o$. For very large z_o, $z_i \approx f$, and we can write the FWHM contribution to the spot diameter as

$$\delta_{\mathrm{source}} = |M|d_o \approx (f/|z_o|)d_o, \tag{79}$$

where d_o is the FWHM of the source.

D. Net Spot Size at the Focus

Rigorously speaking, it is not possible to predict the net spot size from separate calculations of the individual contributions. The aberrations in general interact with one another and with the diffraction and source size effects. Furthermore, in practice one generally wants the net spot size to be at the empirically determined position of smallest focus. This position can be located at the focal plane, the circle of least confusion, or somewhere in between, depending on the relative sizes of the spot size contributions. Nevertheless, an overall sense of the magnitude of the net spot size can be obtained by combining the various contributions in quadrature. In an analysis of a scanning transmission electron-microscope column, this approximation was demonstrated to give the FWHM spot diameter within 10% of the true FWHM as determined by a full wave-optical treatment.[15] The types

Table 1. First-Order Properties of a TEM_{01}* Laser-Atomic Lens for Sodium[a]

Case	v_0 (cm/s)	P_0 (W)	q	f (μm)	z_p (μm)	z_f (μm)	z_f (μm)[b]
A	1×10^4	0.1	3.66	7.04	−11.64	−4.60	−3.9
B	5×10^4	0.1	1.22	9.85	−1.57	8.28	8.4
C	1×10^5	0.1	1.06	30.1	−0.46	29.7	29.9
D	1×10^4	1.0	6.33	11.20	−21.1	−9.86	−7.1
E	5×10^4	1.0	1.60	5.77	−3.57	2.20	2.3
F	1×10^5	1.0	1.18	11.59	−1.30	10.29	10.4

[a] $w_0 = 1.0$ μm, $L = 5.33$ μm, and $p_0 = 2$. f is the focal length of the lens, z_p is the position of the principal plane, and z_f is the position of the focal point for an initially parallel atom beam.
[b] Ref. 6.

of aberration, their relative sizes, and the other spot size contributions in the scanning transmission electron microscope are similar to what is expected for a TEM_{01}* laser atomic lens, so we can assume that the approximation is appropriate in our case as well. Thus, as a general but not a precise measure of the FWHM net spot diameter, we write

$$\delta_{tot} = (\delta_{sph}^2 + \delta_{chr}^2 + \delta_{spont}^2 + \delta_{dip}^2 + \delta_{diffr}^2 + \delta_{source}^2)^{1/2}. \tag{80}$$

The individual FWHM spot sizes are given by Eqs. (45), (54), (69), (76), and (78) and relation (79), respectively.

4. EXAMPLES

Before discussing specific examples, it is perhaps useful to consider the limitations imposed by keeping the lens in the first-order, paraxial regime. As discussed in Subsection 2.A, we require that (a) $r^2 \ll w_0^2$, (b) $p_0 = \mathcal{O}(1)$, (c) $U(r, z) \ll E_0$, and (d) $r' \ll 1$. Given the first two of these requirements, (c) reduces to $\hbar\Delta \lesssim E_0$. This is not much of a limitation on Δ, since $E_0/\hbar$ is usually of the order of 10^{13}–10^{14} rad/s. By examining the slope of the trajectory at the focus, where it reaches its largest value, it can be shown that requirement (d) is satisfied as long as (a) is true. Clearly the most limiting restriction is requirement (a). This is especially true when small spot sizes are desired, since, as is seen below, the ultimate spot size generally decreases as w_0 decreases. Nanometer-sized spot diameters will require small values for w_0, which means the initial atom beam size r_0 will need to be even smaller.

We now discuss some numerical examples in order to provide a general understanding of the operating ranges of the TEM_{01}* laser atomic lens. In all examples we consider the focusing of sodium atoms with a laser tuned near the $3S$–$3P(D_2)$ transition. The wavelength of the transition $\lambda = 0.59$ μm, the natural linewidth $\gamma = 6.28 \times 10^7$ rad/s, and the saturation intensity $I_s = 10$ mW/cm^2. The mass m is 3.84×10^{-23} g. We calculate six cases and also examine the minimum focal length (MFL) condition. The six cases, originally selected by Gallatin and Gould[6] (GG), are chosen with laser powers of 0.1 and 1.0 W for each of three atomic velocities, 1×10^4, 5×10^4, and 1×10^5 cm/s. The laser beam waist w_0 is kept at 1.0 μm, making the Rayleigh length $L = 5.33$ μm, and the detuning is chosen in each case such that $p_0 = 2$.

A. First-Order Properties

Using Eq. (11) for q and Eqs. (18) and (19) for the principal plane locations and focal lengths, it is a simple matter to calculate the first-order lens properties. Table 1 shows the results for the six cases discussed by GG, and Figs. 5(a) and 5(b) show ray traces for each case. In cases A and D we see that $q > 2$, corresponding to a lens with multiple crossovers. The trajectories shown in Fig. 5 illustrate this case. The first principal planes are well removed from the center of the lens, so the lens is quite thick. Case C, on the other hand, is quite close to a thin lens, since the focal length is long and the principal plane is near the lens center. Case E has the shortest focal length of the six cases, and f is close to the minimum value of 5.33 μm. Interestingly, this is true even though q is not close to 2. Apparently there is a relatively wide range of excitations for which the focal length is close to the minimum but the principal plane is in different locations, as can be seen from Fig. 3. This result has design implications in that the minimum focal spot diameter, attained at the shortest focal length for a diffraction limited lens, can be realized over a broad range of excitations.

The last column in Table 1 contains the focal spot locations obtained by GG for a Gaussian atomic beam with a

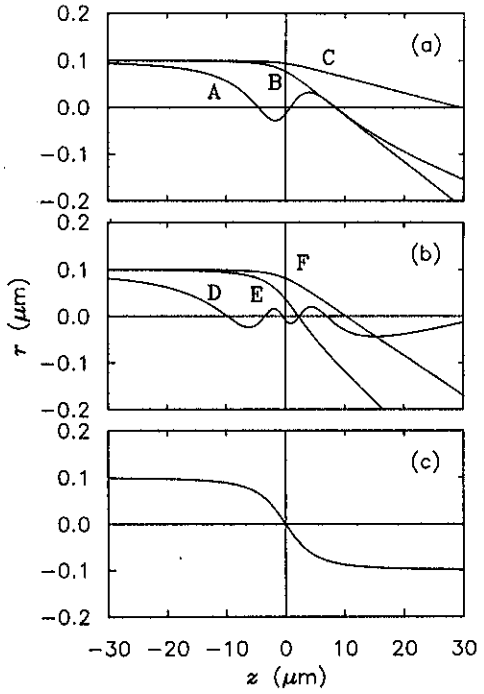

Fig. 5. Ray traces of atomic trajectories through a TEM_{01}* laser atomic lens. (a) Cases A–C of Table 1, $P_0 = 0.1$ W, v_0 is 1×10^4, 5×10^4, and 1×10^5 cm/s, respectively. (b) Cases D–F of Table 1, $P_0 = 1.0$ W, v_0 is 1×10^4, 5×10^4, and 1×10^5 cm/s, respectively. (c) MFL condition with $q = 2$.

Table 2. Laser Power and Detuning Necessary to Achieve MFL Conditions for Three Atomic Velocities[a]

v_0 (cm/s)	P_0^{MFL} (W)	Δ^{MFL} (rad/s)
1×10^4	0.006	1.92×10^{11}
5×10^4	3.68	4.81×10^{12}
1×10^5	58.8	1.92×10^{13}

[a]Results are for sodium atoms with $w_0 = 1.0$ μm and $p_0 = 2$.

waist of radius 0.07 μm located at $z = -3L$. Excellent agreement is seen in all but the thickest-lens cases, A and D, where some deviation is apparent.

The MFL trajectory, the telescopic case, is shown in Fig. 5(c). This situation occurs when $q = 2$, which results in $f = -z_p = L$ (5.33 μm for $w_0 = 1.0$ μm). Given an initial atomic velocity and a fixed p_0 of order 1 (say $p_0 = 2$), the laser power and detuning necessary to achieve the MFL condition are uniquely determined. Using the expression for q [Eq. (11)], we can derive

$$\Delta^{MFL} = \frac{3E_0}{\hbar}\frac{\lambda^2}{\pi^2 w_0^2}, \tag{81}$$

$$P_0^{MFL} = \frac{18}{\pi^3}\frac{E_0^2}{\hbar^2\gamma^2}\frac{\lambda^4}{w_0^2}I_s, \tag{82}$$

where in Eq. (82) we neglect γ in the denominator of Eq. (7). Table 2 shows the laser powers and detunings required for a MFL lens, given the three initial velocities of the examples above. We note that for moderately low atomic velocities the power required is quite small but increases dramatically as the velocity is raised. This effect occurs because P_0^{MFL} depends on E_0^2, resulting in a v_0^4 dependence.

The strong v_0 dependence seen here should not be misinterpreted as causing a large chromatic aberration. It arises because the detuning is increased together with the velocity, requiring more laser power to keep p_0 constant. In a real situation Δ would be held fixed, in which case the chromatic aberration would be as discussed in Subsection 3.B.2.

B. Focal Spot Sizes

In this section we calculate the FWHM spot diameter contributions arising from each of the sources discussed in Section 3, using Eqs. (45), (54), (69), (76), and (78) and relation (79). Results are obtained for the six cases discussed above and also for the MFL condition. An initial beam radius r_0 of 0.1 μm is assumed. For the source size aberration we assume a source of radius 0.1 μm at a distance of 1 cm, which gives a collimation half-angle of 10^{-5}. For the chromatic aberration we assume $\Delta E_{1/2}/E_0 = 2 \times 10^{-3}$, in accord with Refs. 6 and 5. Table 3 shows the results for each spot size contribution in nanometers in each of the six cases as well as the quadrature sum δ_{tot}. Several interesting features are apparent from Table 3. Generally, the largest contributions are diffraction, dipole fluctuations, and spherical aberration. At low initial velocity diffraction is by far the dominant effect, while at high velocities the dipole fluctuations become larger. Spherical aberration is larger at the higher velocities as well, becoming comparable to diffraction in cases C and F. Case E, in which the focal length is shortest, has the smallest net spot size, as expected. The chromatic aberration is quite small in each case; however, this is somewhat arbitrary, since the spot size is proportional to $\Delta E_{1/2}/E_0$. The significance of this is that the restrictions on the fractional energy spread in the atomic beam are not so severe as indicated in earlier reports.[5,6] One part in 10^2 could be tolerated in principle, as this brings the spot size contribution to the same order of magnitude as the other contributions.

To provide a comparison of the diffraction spot size with the results of GG, we also consider the propagation of a Gaussian atomic beam with a waist of radius 0.07 μm located at $z = -3L$. Our results for the $1/e^2$ waist diameters $2\sigma_0$ are given in Table 4 along with those of GG. Interestingly, the spot sizes are in excellent agreement for cases B, C, E, and F. Cases A and D do not show such good agreement. This could be explained perhaps by not-

Table 4. Comparison with GG Values of $1/e^2$ Spot Diameters $2\sigma_0$ for a Gaussian Atomic Beam[a]

Case	$2\sigma_0$	$2\sigma_0$[b]
A	11.0	7.0
B	3.09	3.0
C	4.72	4.7
D	17.3	6.3
E	1.81	1.7
F	1.82	1.8

[a]Diameters are given in nanometers at the focus for the six cases of Table 1; all other spot size contributions are ignored. A waist radius of $\sigma_0 = 0.07$ μm located at $z = -3L = -15.99$ μm is assumed.
[b]Ref. 6.

Table 3. FWHM Spot Diameters (nm) Arising from Each of the Contributions for the Six Cases of Table 1[a]

Case	λ_{dB} (nm)	δ_{sph}	δ_{chrom}	δ_{spont}	δ_{dip}	δ_{diffr}	δ_{source}	δ_{tot}
A	0.172	0.06	0.105	0.087	0.015	7.40	0.14	7.40
B	0.0345	1.11	0.157	0.070	2.32	2.07	0.20	3.32
C	0.0172	1.75	0.184	0.105	5.04	3.17	0.60	6.24
D	0.172	0.02	0.102	0.160	0.001	11.8	0.22	11.8
E	0.0345	0.50	0.129	0.024	0.93	1.21	0.12	1.62
F	0.0172	1.24	0.163	0.032	3.67	1.22	0.23	4.07

[a]Spherical aberration, δ_{sph}; chromatic aberration, δ_{chr}; spontaneous-emission aberration, δ_{spont}; dipole-fluctuation aberration, δ_{dip}; diffraction, δ_{diffr}; source size, δ_{source}. The fractional energy spread in the atomic beam $\Delta E_{1/2}/E_0 = 2 \times 10^{-3}$. The source radius is 0.1 μm, located at $z_o = -1$ cm. δ_{tot} is the quadrature sum of all contributions.

Table 5. FWHM Spot Diameters (nm) at the MFL Condition for Sodium Atoms at Three Atomic Velocities[a]

v_0 (cm/s)	δ_{sph}	δ_{chrom}	δ_{spont}	δ_{dip}	δ_{diffr}	δ_{source}	δ_{tot}
1×10^4	0.27	0.118	0.172	0.18	5.61	0.11	5.63
5×10^4	0.27	0.118	0.016	0.40	1.12	0.11	1.23
1×10^5	0.27	0.118	0.005	0.57	0.56	0.11	0.86

[a]Laser power and detuning are given in Table 2; $w_o = 1.0$ μm, $p_0 = 2$. Spherical aberration, δ_{sph}; chromatic aberration, δ_{chr}; spontaneous-emission aberration, δ_{spont}; dipole-fluctuation aberration, δ_{dip}; diffraction, δ_{diffr}; source size, δ_{source}. The fractional energy spread in the atom beam $\Delta E_{1/2}/E_0 = 2 \times 10^{-3}$. The source radius is 0.1 μm, located at $z_0 = -1$ cm. δ_{tot} is the quadrature sum of all contributions.

ing that the principal plane is located extremely far out of the lens in these two cases. Thus the waist position $z = -3L = -15.99$ μm cannot really be considered to be in a field-free region in these cases, as was assumed by GG.

Spot sizes for the MFL lens are shown in Table 5 for three initial atomic velocities. The laser power and detuning are those given in Table 2. At 1×10^4 cm/s the lens is essentially diffraction limited. At the higher velocities the dipole-fluctuation aberration grows as the contribution from diffraction decreases, so that at a velocity of 1×10^5 cm/s the contributions are approximately equal. The spherical aberration, chromatic aberration, and source size contributions are the same for each velocity because they depend only on parameters held fixed in the MFL lens.

5. LENS OPTIMIZATION

One of the most useful applications of the explicit expressions for the various spot sizes obtained in this paper is lens optimization. By examining how each of the aberrations, diffraction, and the source size contribution depend on the laser- and atomic-beam parameters, it is possible to determine what combinations of parameters give the smallest spot size.

Presuming that a particular atom is chosen, so that the mass m, the wavelength λ, the resonant angular frequency w_0, and the linewidth γ are fixed, there are seven free parameters to be optimized. The laser beam has three parameters available for optimization, i.e., the power P_0, the detuning Δ, and the waist size w_0. Instead of working directly with P_0 and Δ, however, it is more convenient to work with the lens excitation parameter q and the spatially independent saturation parameter p_0. Though these parameters may seem to be interdependent, examination of the definitions shows that, given the freedom to choose any P_0 and Δ, any values for q and p_0 can be obtained.

The atomic beam has four parameters that can in principle be selected for minimum spot size: the source size d_o, the beam radius at the lens r_0, the mean velocity v_0, and the energy spread $\Delta E_{1/2}$.

Of the seven parameters available for optimization, three can be identified as not having specific values that minimize any of the spot size contributions. The parameter p_0 has no effect on chromatic aberration, diffraction, or the source size effect, and its effect on the spherical, spontaneous, and dipole aberrations is to reduce them monotonically as it decreases. The source size d_o affects only the source size contribution, which is directly proportional to it. The energy width $\Delta E_{1/2}$ is similar in that it has only a linear effect on the chromatic aberration. To obtain the smallest possible spot size, the only option is to make these three parameters as small as practically possible or small enough so that the contribution to the total spot size is negligible.

The remaining four parameters, q, w_0, r_0, and v_0, affect the spot size contributions in different ways, causing some to increase and others to decrease and having no effect on others. Thus it is reasonable to ask which values of these parameters give the smallest spot size.

First, let us examine the behavior of the net spot size as a function of the lens excitation q. All the aberrations, with the exception of the chromatic, can be made arbitrarily small with sufficiently large q. The chromatic aberration decreases initially but becomes constant for large enough q. The diffraction and source size contributions to the spot size, however, are smallest at the MFL condition $q = 2$. Since diffraction and the source size are major contributions to δ_{tot} at the smallest spot sizes, it seems reasonable to choose $q = 2$ as an optimum value. Additionally, this gives the lens symmetry properties; i.e., the focal spot is at the center of the lens, which could be important for practical reasons.

Let us now let $q = 2$ and ask how the total spot size at the MFL can be minimized with respect to w_0, r_0, and v_0. The source size contribution is not affected by any of these three parameters, so we can ignore it for the present discussion. With $q = 2$ the remaining FWHM spot diameters can be written as

$$\delta_{sph} \approx \frac{9\pi}{1024}(p_0 + 8)\frac{r_0^3}{w_0^2}, \tag{83}$$

$$\delta_{chr} = \frac{3\pi}{16}\frac{\Delta E_{1/2}}{E_0} r_0, \tag{84}$$

$$\delta_{spont} = \frac{\pi^{5/2}}{2}\left(\frac{\ln 2}{6}\right)^{1/2}\left(\frac{\gamma p_0}{\lambda^5}\right)^{1/2}\frac{h}{m}\frac{w_0^2 r_0}{v_0^{3/2}}, \tag{85}$$

$$\delta_{dip} = \frac{3(91 \ln 2)^{1/2}}{256} p_0 \left(\frac{\lambda}{\gamma}\right)^{1/2}\frac{r_0^3}{w_0^3} v_0^{1/2}, \tag{86}$$

$$\delta_{diffr} = 0.61\pi \frac{h}{m\lambda}\frac{w_0^2}{r_0 v_0}, \tag{87}$$

where the spherical-aberration spot size is approximated by only the first term in Eq. (45). This is a good approximation, because L is generally larger than w_o. With relation (83) and Eqs. (84)–(87), we can write the square of the total spot size as

$$\delta_{tot}^2 = A\frac{r_0^6}{w_0^4} + Br_0^2 + C\frac{w_0^4 r_0^2}{v_0^3} + D\frac{r_0^6 v}{w_0^6} + E\frac{w_0^4}{r_0^2 v_0^2}, \quad (88)$$

with

$$A = \left[\frac{9\pi}{1024}(p_0 + 8)\right]^2, \quad (89)$$

$$B = \left[\frac{3\pi}{16}\frac{\Delta E_{1/2}}{E_0}\right]^2, \quad (90)$$

$$C = \frac{\pi^5 \ln 2}{24}\frac{\gamma p_0}{\lambda^5}\frac{h^2}{m^2}, \quad (91)$$

$$D = \frac{819 \ln 2}{65536}\frac{\lambda}{\gamma}p_0^2, \quad (92)$$

$$E = 0.372\pi^2\frac{h^2}{m^2\lambda^2}. \quad (93)$$

Optimizing the lens for minimum spot size now consists of minimizing Eq. (88) with respect to the three free parameters w_0, r_0, and v_0. This calculation is best done numerically, especially since in any real situation there will be constraints imposed on these parameters. For three simple examples we consider a base case with $\delta_{source} = 0.11$ nm, $p_0 = 2$, $\Delta E_{1/2}/E_0 = 2 \times 10^{-3}$, $w_0 = 1.0$ μm, $r_0 = 0.1$ μm, and $v_0 = 5 \times 10^4$ cm/s (i.e., the second case in Table 5). We let each of the three parameters vary in turn while keeping the other parameters fixed. When w_0 is free, a minimum spot of 1.11 nm is obtained at $w_0 = 0.867$ μm. Allowing r_0 to vary gives a minimum of 1.21 nm at $r_0 = 0.107$ μm. Varying v_0 gives a minimum spot diameter of 0.835 nm with $v_0 = 1.25 \times 10^5$ cm/s. These values show that the arbitrarily chosen examples in Section 4 are fairly close to optimal.

6. CONCLUSION

We have shown that a TEM_{01}* laser atomic lens can act as a focusing optical element for an atomic beam with high resolution. By using particle-optics techniques, we have derived simple expressions for the first-order properties of the lens and also for all the major aberrations that contribute to the spot size of a focused atomic beam. Diffraction and source size contributions to the spot size have been determined as well, and various examples have been discussed. With the expressions derived in this paper optimization of the lens is shown to be possible.

Our main purpose in this paper has been to provide a detailed description of the TEM_{01}* laser atomic lens so that any future experimental work on such a lens will have a solid basis to build on. If attained experimentally, the focal spot sizes of ~1 nm discussed in this paper will open a wealth of new possibilities for nanostructure research, microscopy, and precision measurements. Although achieving some of the laser- and atomic-beam parameters required for these spot sizes may push the limits of present technology, it is likely that in the near future these parameters will be realizable.

ACKNOWLEDGMENTS

We thank the members of the Electron Physics Group at the National Institute of Standards and Technology, in particular Mark D. Stiles for stimulating conversations and Joseph A. Stroscio for assistance in generating Figure 1.

*Present address, Center for Solid State Science, Arizona State University, Tempe, Arizona.

REFERENCES

1. J. E. Bjorkholm, R. R. Freeman, A. Ashkin, and D. B. Pearson, Phys. Rev. Lett. **41,** 1361 (1978).
2. J. E. Bjorkholm, R. R. Freeman, A. Ashkin, and D. B. Pearson, Opt. Lett. **5,** 111 (1980).
3. V. I. Balykin, V. S. Letokhov, Yu. B. Ovchinnokov, and A. I. Sidorov, J. Mod. Opt. **35,** 17 (1988).
4. J. P. Gordon and A. Ashkin, Phys. Rev. A **21,** 1606 (1980).
5. V. I. Balykin and V. S. Letokhov, Opt. Commun. **64,** 151 (1987).
6. G. M. Gallatin and P. L. Gould, J. Opt. Soc. Am. B **8,** 502 (1991).
7. W. Glaser, Z. Phys. **117,** 285 (1941); see also Ref. 9 below.
8. See, e.g., H. Goldstein, *Classical Mechanics* (Addison-Wesley, Reading, Mass., 1950).
9. P. Grivet, *Electron Optics,* 2nd ed. (Pergamon, Oxford, 1972).
10. P. W. Hawkes and E. Kasper, *Electron Optics* (Academic, London, 1989), Vol. 1.
11. See also, e.g., A. B. El-Kareh and J. C. J. El-Kareh, *Electron Beams, Lenses, and Optics* (Academic, New York, 1970), Vol. 2; M. Szilagyi, *Electron and Ion Optics* (Plenum, New York, 1988).
12. See, e.g., J. Mathews and R. L. Walker, *Mathematical Methods of Physics* (Benjamin, Menlo Park, Calif., 1964), p. 8.
13. See, e.g., R. K. Pathria, *Statistical Mechanics* (Pergamon, Oxford, 1972), pp. 456*ff.*
14. J. Dalibard and C. Cohen-Tannoudji, J. Opt. Soc. Am. B **2,** 1707 (1985).
15. M. Scheinfein and M. Isaacson, J. Vac. Sci. Technol. B **4,** 326 (1986); M. Scheinfein, "Transmission electron energy loss spectroscopy at 5Å spatial resolution," Ph.D. dissertation (Cornell University, Ithaca, N.Y., 1985).